# EFFECT OF ASPECT RATIO ON COUPLED SOLUTE-THERMOCAPILLARY CONVECTION INSTABILITY IN HALF-ZONE LIQUID BRIDGE

by

***Yong ZOU[a*], Hulin HUANG[b], Shoujun DING[a], Xianshan HUANG[a], Jianjun MA[a], and Hongmei CHEN[a]***

[a] School of Mathematics and Physics, Anhui University of Technology, Ma'anshan, China
[b] College of Astronautics, Nanjing University of Aeronautics and Astronautics, Nanjing, China

Original scientific paper
https://doi.org/10.2298/TSCI210611104Z

*Floating zone method is an important technology for growth of high integrity and high uniformity single crystal materials due to its free of crucible contamination. However, capillary convection in the melt is a great challenge to floating zone crystal growth. In this paper, numerical simulations are performed to investigate the coupled solute-thermocapillary convection in $Si_xGe_{1-x}$ system of the half-zone liquid bridge. The impact of aspect ratio, As, is also investigated on stability of capillary convection. For As = 0.5, the results show that pure solute capillary convection is very weak, which presents 2-D axisymmetric structure. The temperature field is mainly determined by thermal diffusion, while the concentration field is dominated by convection and solute diffusion together. Coupled solute-thermocapillary convection exhibits 3-D periodic and rotating oscillatory flow with the azimuthal wavenumber m = 4, while the pure thermocapillary convection presents a 3-D steady non-axisymmetric flow while solute capillary convection is absent. This means that instability of convection will increase when two kinds of capillary convection are coupled. When the height of the liquid bridge is changed from 5 mm to 10 mm with a constant radius of 10 mm, azimuthal wavenumber, m, of coupled capillary convection shows a strong dependence on aspect ratio. The relationship between the azimuthal wavenumber and aspect ratio can be written as $m \times As = 2$ or $m \times As = 2.2$. Further results indicated that when velocity of the monitoring point is large, corresponding concentration is also high at that moment, but the phases of concentration and velocity are not completely synchronized.*

Key words: *numerical simulation, coupled solute-thermocapillary convection, aspect ratio, floating zone technique*

## Introduction

Floating zone method is a promising technique to growth single crystals with the advantage of containerless environment, which is widely used for the growth of high precision silicon, super alloys and other semiconductor material [1-3]. Marangoni convection driven by surface tension gradient has a dramatic effect on distribution of impurity concentration in melt, due to existence of free surface in floating zone growth system [4, 5]. Experimental [6-9] and theoretical [10-13] researches including linear stability analyses and non-linear direct numerical simulations have been carried out in depth on stability of pure thermocapillary convection.

* Corresponding author, e-mail: yong.zou@163.com

The results show that Marangoni convection will be unstable and thermal fluid wave instability will occur with increasing temperature difference. With the temperature difference further increased, more complex oscillatory flow will appear which is related to Marangoni number. It is found that traveling waves will occur in the flow field near critical Marangoni number and flow pattern will also change with aspect ratio. The continuously increasing Marangoni number will cause the flow to enter chaotic state.

In fact, there is a large concentration gradient in the melt during floating zone growth, due to the doping demand of semiconductor crystals, especially alloy materials. This will cause strong macrosegregation. Concentration gradient at the surface induces solute capillary convection, which is coupled with thermocapillary convection generated by temperature gradient to form a complex flow. By using linear stability method, Lyubimova *et al.* [14, 15] analyzed development of 3-D thermo-solute coupled convection under different conditions in floating zone growth, and obtained characteristics and structural images of non-axisymmetric convection evolution with time. They found that existence of weak thermocapillary effect will have a great influence on stability of solute convection, and *vs*. Minakuchi *et al.* [16] studied thermo-solute coupled capillary convection under zero gravity with a full-floating liquid bridge model. It was concluded that although the $Ma_C$ number is larger than $Ma_T$ number, axial convection intensity caused by concentration gradient on the free surface is smaller than thermocapillary convection. Later, the research team of Minakuchi *et al.* [17, 18] further studied the half-floating zone model. The results show that when solute capillary force and thermal capillary force act together, the critical Marangoni number of the coupled capillary convection is larger than that of pure solute capillary force. At the same time, when thermo-solute capillary convection coexists, azimuthal wavenumber of liquid bridge is significantly affected. Surovovs *et al.* [19] used open source software OpenFOAM to simulate melt flow, temperature and impurity concentration fields, and then compared the crystal interface and resistivity distribution of the obtained crystals with the experimental results. Furthermore, the influence of Marangoni number on the flow velocity field of the melt was analyzed. Zhou and Huai [20] performed numerical analysis on thermocapillary convection and solute capillary convection in a liquid bridge with variable interfaces. It was found that when $Ma_T/Ma_C = -1$, the free surface is convex at both ends of cold and hot and contracted in the middle. In order to understand the characteristics of pure solutocapillary flow, Chen *et al.* [21] performed a series of 3-D numerical simulations in a shallow annular pool subjected to a constant radial solutal gradient. Results indicate that solutocapillary flow is steady and axisymmetric at a small solutal capillary Reynolds number. With increase of solutal capillary Reynolds number, 3-D oscillatory flow is observed. Huang *et al.* [22] analyzed effect of thermocapillary convection in liquid bridge on impurity diffusion. Numerical results show that impurity distribution in melt is anisotropic under influence of thermal capillary convection. Impurity concentration contour on meridian plane is dumbbell shaped, while concentration contour on cross-section is star-shaped. Moreover, radial segregation effect increases with increment of Marangoni number. Mendis *et al.* [23] found that aspect ratio affects both the critical thermal Marangoni number and critical solutal Marangoni number drastically.

Theoretically, complex flow driven by multi-force coupling in melt belongs to multiparameter flow instability problem. There are many factors that affect flow structure and its stability, and the driving force levels are similar and coupled with each other [24, 25]. Small change of some parameters will cause change of flow stability and dissipation structure. So far, numerical study focusing on coupled capillary convection is still insufficient, and some results are contradictory [14, 15, 17]. In addition, in view of difficulties in theoretical analysis and experimental research under high temperature conditions, only a small number of experiments

reported adverse effects of solute capillary convection on silicon and germanium (Si-Ge) floating crystal growth [26]. The Si-Ge mixed crystals have a wide range of applications in microelectronic and optoelectronic devices such as photo-detectors, solar cells, optical switches, and power generators [26, 27]. Moreover, hexagonal Si-Ge alloy embodies an ideal material system in which to combine electronic and optoelectronic functionalities on a single chip [28]. In all these applications, the compositional uniformity of grown crystals is important. In this paper, the half-floating liquid bridge is used to study contribution of thermocapillary force and solute capillary force to coupled convection in $Si_xGe_{1-x}$ system (a mixture of Si-Ge) by numerical simulation. Characteristics of various capillary convections and heat and mass transfer in melt under different aspect radios are compared and analyzed.

## Mathematical and physical models

In this paper, half-zone liquid bridge in the cylindrical co-ordinate system ($r$, $\theta$, $z$) is used as shown in fig. 1. Under zero gravity, we have not taken into account deformation of free surface to simplify the model. Under this condition, following assumptions are used in the model:

- free surface of the liquid bridge remains cylindrical,
- height of the liquid bridge is $L$, and the liquid bridge is suspended between the disks with same radius, $R$, and
- solid-liquid interfaces located at $z = L/2$ and $z = -L/2$, respectively are simplified to non-slip planes, which temperature difference $\Delta T$ ($\Delta T = T_h - T_c$) remains unchanged.

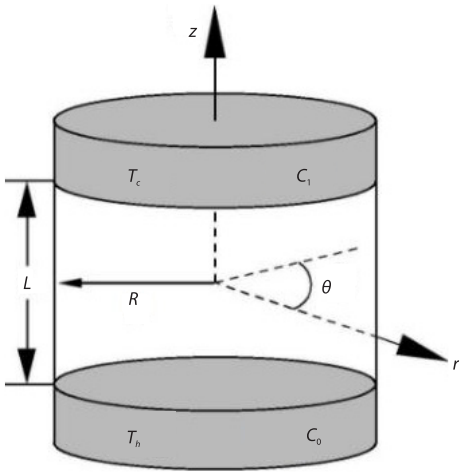


**Figure 1. Physical model**

Assuming that melt is incompressible Newtonian viscous fluid mixture, surface tension acting on the free surface can be expressed as a linear function of temperature and concentration [20]:

$$\sigma = \sigma_0 + \gamma_T (T - T_0) + \gamma_C (C - C_0) \tag{1}$$

where

$$\sigma_0 = \sigma(T_0, C_0),\ \gamma_T = \frac{\partial \sigma}{\partial T},\ \gamma_C = \frac{\partial \sigma}{\partial C}$$

In this study we only consider the case that surface tension decreases with increase of temperature and increases with increase of solute concentration. It is assumed that other physical properties of the fluid do not change with temperature but only change with concentration, and show a simple linear mixing law with concentration.

For incompressible fluid, governing equations in the melting zone can be expressed:

- Continuity equation

$$\frac{\partial \rho}{\partial t} + \nabla(\rho \mathbf{V}) = 0 \tag{2}$$

- Momentum equation

$$\frac{\partial(\rho \mathbf{V})}{\partial t} + (\mathbf{V}\nabla)(\rho \mathbf{V}) = -\nabla P + \nabla(\mu \nabla)\mathbf{V} \tag{3}$$

– Energy equation

$$\frac{\partial(\rho T)}{\partial t}+(\mathbf{V}\nabla)(\rho T)=\nabla\left(\frac{\kappa}{c_p}\nabla T\right) \tag{4}$$

– Concentration equation

$$\frac{\partial C}{\partial t}+(\mathbf{V}\nabla)C=D\nabla^2 C \tag{5}$$

where **V**, $P$, $T$, and $C$ are velocity, pressure, temperature, and silicon concetration, respectively. In addition, $\rho$ is the density, $\mu$ – the kinematic viscosity, $\kappa$ – thermal conductivity, $c_p$ – the specific heat, and $D$ – diffusion coefficient of Si in Ge, respectively. Assuming that physical properties of mixed melt have a simple linear relationship with concentration of Si, they can be represented [29]:

$$\rho=C\rho_{\mathrm{Si}}+(1-C)\rho_{\mathrm{Ge}},\ \mu=C\mu_{\mathrm{Si}}+(1-C)\mu_{\mathrm{Ge}},\ \kappa=C\kappa_{\mathrm{Si}}+(1-C)\kappa_{\mathrm{Ge}},\ c_p=Cc_{p\mathrm{Si}}+(1-C)c_{p\mathrm{Ge}}$$

where subscripts of Si and Ge identify silicon and germanium.

**Table 1. Physical properties of $Si_xGe_{1-x}$ melt and other parameters needed**

| Property | Symbol | Value |
|---|---|---|
| Density [kgm$^{-3}$] | $\rho_{\mathrm{Si}}/\rho_{\mathrm{Ge}}$ | $2.52\cdot10^3/5.51\cdot10^3$ |
| Dynamic viscosity [kgm$^{-1}$s$^{-1}$] | $\mu_{\mathrm{Si}}/\ \mu_{\mathrm{Ge}}$ | $7\cdot10^{-4}/7.4\cdot10^{-4}$ |
| Thermal conductivity [Wm$^{-1}$K$^{-1}$] | $\kappa_{\mathrm{Si}}/\ \kappa_{\mathrm{Ge}}$ | 64/50 |
| Specific heat [Jkg$^{-1}$K$^{-1}$] | $c_{p\mathrm{Si}}/c_{p\mathrm{Ge}}$ | $1\cdot10^3/0.4\cdot10^3$ |
| Thermal diffusion coefficient [ m$^2$s$^{-1}$] | $\alpha_{\mathrm{Si}}/\alpha_{\mathrm{Ge}}$ | $2.54\cdot10^{-5}/2.27\cdot10^{-5}$ |
| Surface tension gradient [Nm$^{-1}$K$^{-1}$/Nm$^{-1}$] | $\gamma_T/\gamma_C$ | $-7\cdot10^{-5}/2.57\cdot10^{-5}$ |
| Prandtl number [–] | $\mathrm{Pr_{Si}}/\mathrm{Pr_{Ge}}$ | 0.011/0.006 |
| Schmidt number [–] | $\mathrm{Sc_Si}/\mathrm{Sc_{Ge}}$ | 28/13 |
| Diffusion coefficient [m$^2$s$^{-1}$] | $D$ | $1\cdot10^{-8}$ |
| Length of float zone [m] | $L$ | 0.005, 0.0075, 0.01 |
| Radius of float zone [m] | $R$ | 0.01 |
| Temperature of upper-disc [K] | $T_h$ | 1310 |
| Temperature of lower-disc [K] | $T_c$ | 1300 |
| Temperature difference [K] | $\Delta T$ | 10 |
| Si concentration of upper-disc [–] | $C_1$ | 1 |
| Si concentration of lower-disc [–] | $C_0$ | 0 |

Boundary and initial conditions are set:

Upper-disc ($z = L/2$): non-slip and fixed temperature $T = T_c$, and the melt concentration $C = C_1 = 1$ (6a)

Lower-disc ($z = -L/2$): non-slip and fixed temperature $T = T_h$, and the melt concentration $C = C_0 = 0$ (6b)

Free surface ($r = R$): Along the free surface impervious to flow of mass and energy:

$$\frac{\partial T}{\partial r} = \frac{\partial C}{\partial r} = 0$$

and following tangential force balance for Marangoni convection:

$$-\mu \frac{\partial \mathbf{V}}{\partial \mathbf{n}} = \gamma_T \nabla T + \gamma_C \nabla C \tag{6c}$$

where **n** is unit normal vector of the free surface.

Initial conditions are expressed as ($t = 0$): no flow (zero flow velocity) and prescribed constant temperature $T = \frac{\Delta T}{2}$ and constant concentration $C = \frac{1}{2}$ (6d)

Prandtl and Schmidt numbers, aspect radio and dimensionless temperature are defined as $\mathrm{Pr} = \nu/\alpha$, $\mathrm{Sc} = \nu/D$, $As = L/\mathrm{R}$, and $T^* = (T - T_c)/\Delta T$. Effects of thermocapillary force and solute capillary force are characterized by using thermal Marangoni number $\mathrm{Ma}_T = -(\gamma_T \Delta TL)/\mu\alpha$ and solutal Marangoni number $\mathrm{Ma}_C = -(\gamma_C \Delta CL)/\mu\alpha$, respectively. Physical parameters of $Si_xGe_{1-x}$ system [26, 27] and other parameters needed are listed in tab. 1.

## Numerical method

The finite volume method is used to discretize governing equations on structured grids. Finer mesh gradation is utilized in the regions near the upper and lower disks, as well as the free surface. All numerical results are checked for grid independency. For $As = 0.5$, grid independence verification curve is shown in fig. 2, and corresponding grid amounts are shown in tab. 2. Figure 2 suggests little change of the maximum values of dimensionless temperature $T^*_{\max}$ at the monitoring point ($r = R$, $\theta = 0$, $z = 0$) in the liquid bridge when the grid amount is larger than $2 \cdot 10^5$. Considering accuracy and efficiency of calculation, the grid of $40^r \times 80^\theta \times 80^z$ is finally selected for numerical calculation with a time step of $10^{-3}$ seconds. Convection terms, diffusion terms and time terms are discretized by QUICK scheme, the second-order central difference and the second-order implicit propulsion method, respectively. The PISO algorithm is used for pressure-velocity coupling and all simulations are completed by ANSYS FLUENT 19.0. The numerical method has been verified by comparing the maximum velocity $v_{\max}$ and the maximum circumferential velocity $w_{\max}$ for Pr = 0.01 and Re = 3500 from [30] in the same half-liquid bridge. Details can be found in literature [31].

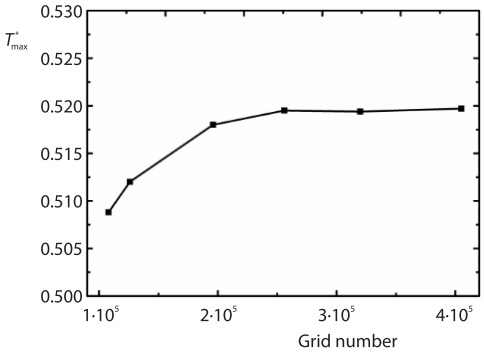


**Figure 2. Grid independence verification curve**

**Table 2. Grid numbers with different meshes**

| Mesh | $30^r \times 60^\theta \times 60^z$ | $30^r \times 60^\theta \times 70^z$ | $40^r \times 70^\theta \times 70^z$ | $40^r \times 80^\theta \times 80^z$ | $50^r \times 80^\theta \times 80^z$ | $50^r \times 90^\theta \times 90^z$ |
|---|---|---|---|---|---|---|
| Grid number | $1.08 \cdot 10^5$ | $1.26 \cdot 10^5$ | $1.96 \cdot 10^5$ | $2.56 \cdot 10^5$ | $3.20 \cdot 10^5$ | $4.05 \cdot 10^5$ |

## Results and discussion

### *Capillary convection characteristics in the liquid bridge*

Temperatures of upper and lower walls are set to $T_c$ = 1300 K and $T_h$ = 1310 K ($\Delta T = T_h - T_c$ = 10 K), respectively. Radius and height of the liquid bridge are set to $R$ = 10 mm and $L$ = 5 mm. Surface tension gradient $\gamma_T = -7 \cdot 10^{-5}$ N/mK and $\gamma_C = 2.57 \cdot 10^{-5}$ N/m, respectively.

When only pure solute capillary force is considered, convection driven by it flows along the free surface from the bottom surface with lower Si concentration the upper surface with higher concentration. Therefore, two symmetrical convection vortices are formed in the meridional plane, and correspondingly, a pair of back-flow vortices is formed in the central region of the liquid bridge. Convection driven by thermocapillary force flows along the free surface also from the bottom surface with lower temperature to the upper surface with higher temperature. Both solute capillary convection and thermocapillary convection flow along the free surface from the bottom to the upper, and the flow are enhanced as they couple.

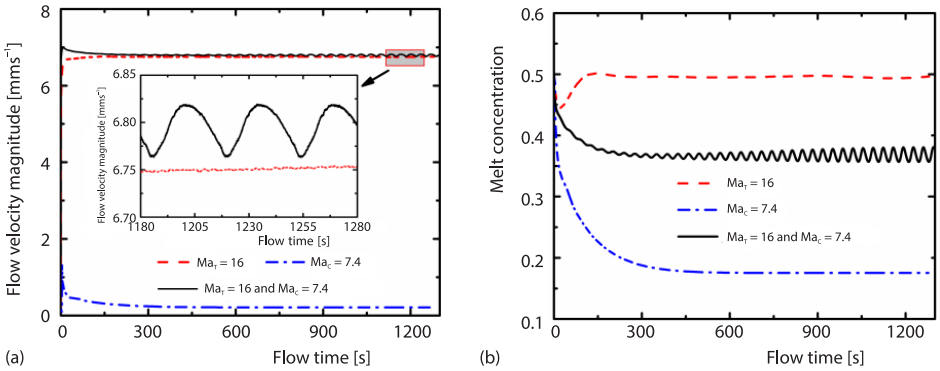


**Figure 3. Time-varying curves of velocity and Si concentration at the monitoring point *p*; (a) flow velocity *vs.* flow time and (b) Si concentration *vs.* flow time**

Figure 3 shows the time-varying curves of velocity and Si concentration at the monitoring point $p(r = R, \theta = 0, z = 0)$. It can be seen from fig. 3(a) that velocity of $p$-point is small with value of $V_1$ = 0.21 mm/s when melt is driven only by solute capillary force, while velocity of $p$-point is large with value of $V_2$ = 6.75 mm/s when driven by the thermocapillary force. Since solute capillary convection is very weak, intensity of coupled capillary convection and that of thermocapillary convection are comparable when two different forms of convection are superimposed. However, driven by both solute capillary force and thermocapillary force, melt convection presents a 3-D periodic oscillation mode. This indicates that flow stability changes. Figure 3(b) exhibits that solute capillary convection has a great influence on concentration at the surface. Although intensity of thermocapillary convection is stronger than that of solute capillary convection, concentration of Si at $p$-point driven by solute capillary convection is much lower than that driven by thermocapillary convection. The melt concentration of $p$-point after coupling changes periodically with time. Its average value is contributed by both thermocapillary convection and solute capillary convection, respectively. Fourier spectrum analysis shows that frequency of solute oscillation is same as that of velocity oscillation with value $f$ = 0.0302 Hz ($\tau$ = 33.1 seconds). Velocity exhibits a small oscillation mode, while concentration in the melt undergoes a large oscillation. It is predicted that even weak solute convection will cause a large change of stability of thermocapillary convection, and steady-state convection will be convert-

ed into periodic oscillating convection. This conclusion can be verified by Lyubimova *et al.* [14, 15].

Further, fig. 4 shows velocity profile of the middle section $z = 0$ at a certain instant. Convection in the liquid bridge transforms from 2-D axisymmetric flow to 3-D steady-state non-axisymmetric flow with azimuthal wavenumber $m = 4$. Both are driven by solute capillary force and thermocapillary force, respectively. Azimuthal wavenumber of capillary convection after superposition is also $m = 4$. It should be mentioned here that concentration on $z = 0$ has similar distribution with that of velocity with same azimuthal wavenumber $m = 4$.

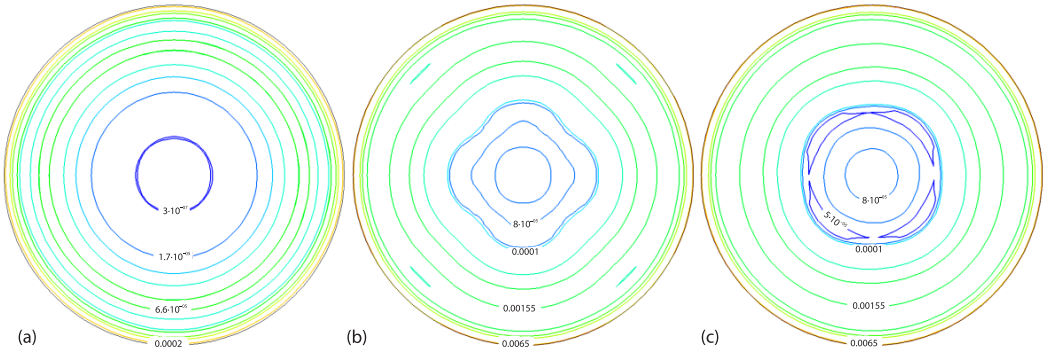


**Figure 4. Velocity distribution [ms$^{-1}$] of the middle section $z = 0$ at certain instant; (a) solute capillarity convection, (b) thermocapillary convection, and (c) coupled capillary convection**

*Effect of aspect radio on coupled capillary convection*

Radius of the liquid bridge is set to $R = 10$ mm and kept constant. Height $L$ of the liquid bridge is used from 5-10 mm. Thus the value of aspect ratio is in the region from 0.5-1. Other parameters of the liquid bridge are kept constant.

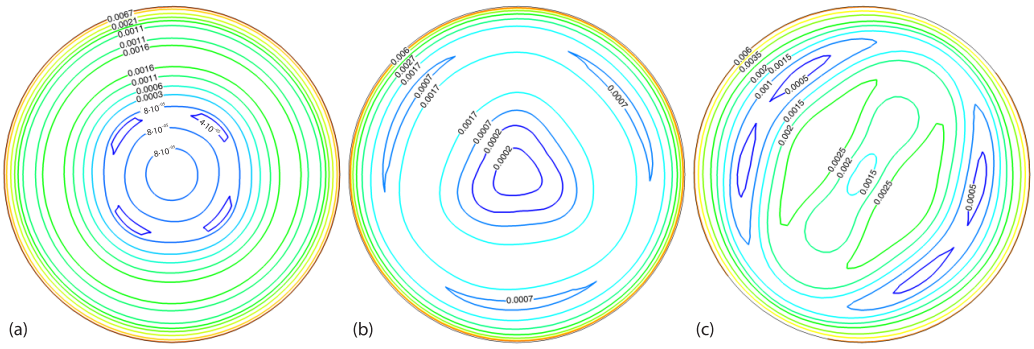


**Figure 5. Velocity distribution at $z = 0$ with different aspect ratio; (a) $As = 0.5$, (b) $As = 0.75$, and (c) $As = 1$**

Figure 5 shows velocity distribution at $z = 0$ with different aspect ratio. As shown in fig. 5, flow velocity inside the liquid bridge is less than that near the free surface. The maximum velocity appears near the surface, but the minimum velocity does not appear in the center of section. Velocity distributions are all central, rotational and symmetrical. The melt flow presents a 3-D convection structure with azimuthal wavenumber $m$ change with aspect ratio. When aspect ratio are 0.5, 0.75, and 1, respectively, corresponding azimuthal wavenumbers $m$ are 4, 3, and 2. The relationship between azimuthal wave number $m$ and aspect ratio of the liquid bridge can be written:

$$As \times m \approx 2 \quad \text{or} \quad As \times m \approx 2.2 \tag{7}$$

For liquid bridge with $As \leq 1$, relationship between aspect ratio and $m$ has same explanation of pure themocapillary convection [32, 33]. Based on idea advanced by Preisser *et al.* [32] that scale of axial mainstream vortex is approximately equal to height of the liquid bridge, it is reasonable that size of the azimuthal wave is equal to size of basic flow vortex in the axial direction of the liquid bridge. Equation (7) is only an approximate relation. When aspect ratio is very small, values of $m$ calculated by eq. (7) do not match well with the calculated result. Thus, this explanation needs to be further verified.

Figure 6 shows temperature distribution at $z = 0$, which are rotational and symmetrical. It is similar to velocity distribution. In the radial direction, temperature is raised, however with influence of internal circumfluence the region with the lowest temperature does not lay at the center of the section. Temperature difference on the section increases with increase of aspect ratio. For the liquid bridge with $As = 0.5$, four symmetrical hot and cold regions are formed on the free surface. For the liquid bridge with $As = 0.75$, three hot and three cold regions are formed on the free surface. For the liquid bridge of $As = 1$, two hot and cold regions are formed on the free surface. Accordingly, the lowest temperature centers are formed in the liquid bridge which numbers are 4, 3, and 2. In other words, the azimuthal temperature wavenumbers $m$ are 4, 3, and 2, respectively.

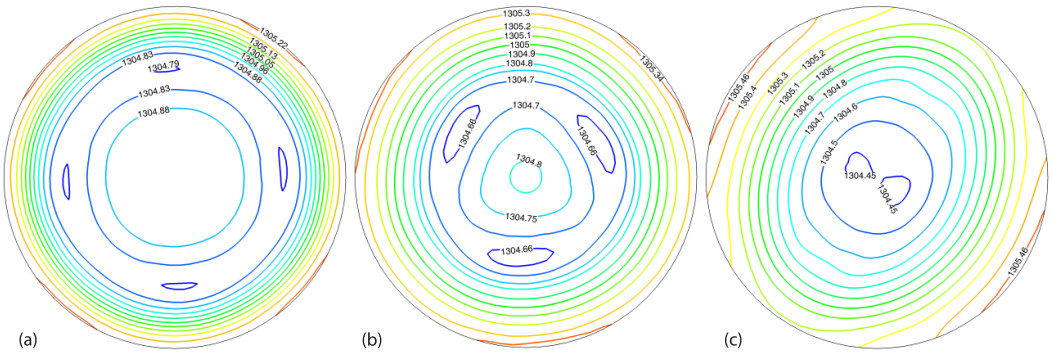


**Figure 6. Temperature distribution at $z = 0$ with different aspect ratio; (a) $As = 0.5$, (b) $As = 0.75$, and (c) $As = 1$**

Under effect of convection in the liquid bridge, Si concentration distribution in the melt is also 3-D. Figure 7 shows that Si concentration distribution is also rotational and symmetric, and azimuthal wavenumber of Si concentration is same as velocity azimuthal wavenumber. When aspect ratio increases from 0.5-1, azimuthal wavenumber $m$ of Si concentration is 4, 3, and 2 at three different aspect ratios, respectively.

Figure 8 shows velocity streamline distribution on the meridian plane $\theta = \pi/2$. At $As = 0.5$, a pair of coupled solute-thermocapillary convection vortices are formed in outer region of the liquid bridge, and a pair of reverse reflux vortices are formed in inner region. When aspect ratio is increased to 0.75, height of the liquid bridge increases and axial scale of the coupled capillary convection vortices increases. According to Preisser *et al.* [32] opinion capillary convection vortices should present a round shape on the meridian plane, and then size of capillary convection vortices would also increase in the radial direction. This would cause the reverse reflux vortex to be squeezed near central axis of the liquid bridge. The result shows that development of the reverse reflux vortex inside the liquid bridge is not complete. When aspect ratio is 1, the surface tension flow fills entire meridian plane, and the reflux vortex inside

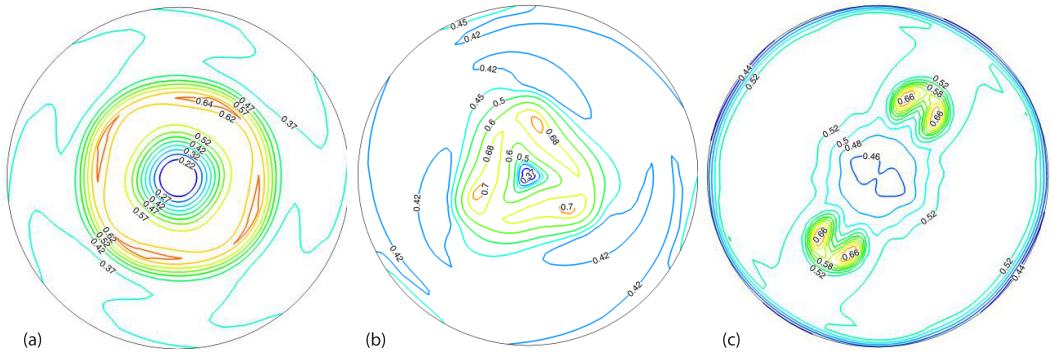


**Figure 7. The Si concentration distribution at $z = 0$ with different aspect ratio; (a) $As = 0.5$, (b) $As = 0.75$, and (c) $As = 1$**

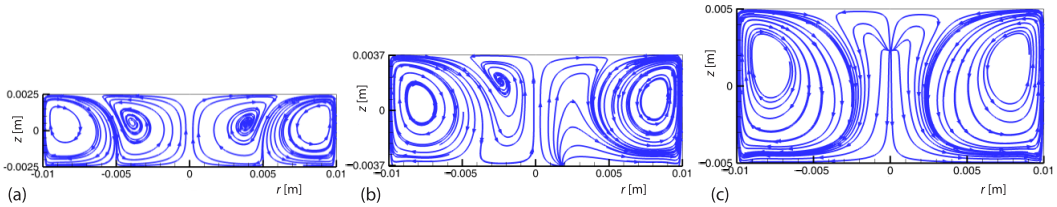


**Figure 8. Velocity streamline distribution on meridian plane $\theta = \pi/2$; (a) $As = 0.5$, (b) $As = 0.75$, and (c) $As = 1$**

the liquid bridge disappears. The numerical results show that the maximum axial velocity of the surface is located near the bottom surface of the liquid bridge under three different aspect ratios. The distance from the position where the maximum velocity occurs to the bottom surface is 30% of height of the liquid bridge.

Figure 9 indicates temperature distribution on the meridian plane $\theta = \pi/2$. For low-Pr fluids, heat diffusion capacity is larger than that of momentum diffusion, so it can be seen from figures that temperature isolines on the meridian plane are generally flat. Near the free surface, isotherms are approximately perpendicular to the free surface, while in most areas inside the liquid bridge, temperature isolines are roughly parallel to the bottom surface and upper surface. Hot fluid is transported to the cold end along the free surface, and then cold fluid is transported from the inside of the melt to the hot end to complete reflux. Therefore, temperature gradient near the corners at the bottom is smaller than that near the corners at the upper, meanwhile temperature gradient inside the melt near the hot wall at bottom is larger than that near the cold wall at upper. This phenomenon is pronounced as aspect ratio increases. It should be noted that since temperature difference between the upper and lower surfaces of the liquid bridge is the same under different aspect ratios. The larger aspect ratio, the smaller average axial temperature gradient.

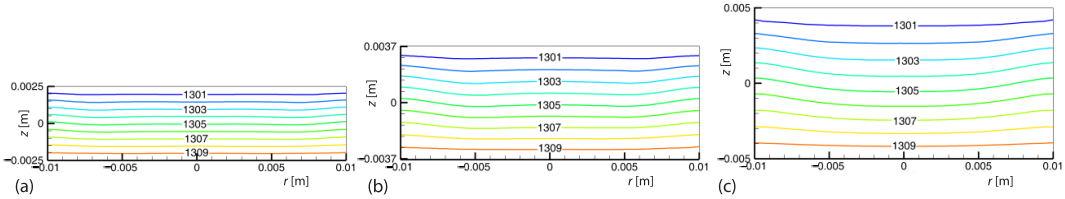


**Figure 9. Temperature distribution on the meridian plane $\theta = \pi/2$; (a) $As = 0.5$, (b) $As = 0.75$, and (c) $As = 1$**

The Si concentration distribution on the meridian plane $\theta = \pi/2$ is different with aspect ratio, as shown in fig. 10. In general, Si concentration value in most regions of the melt is between 0.4 and 0.5, while concentration gradient near the upper and lower surfaces is larger. Comparing with fig. 9, it is found that concentration distribution is closely related to melt velocity and flow direction, and the characteristics of concentration distribution are significantly different from that of temperature distribution.

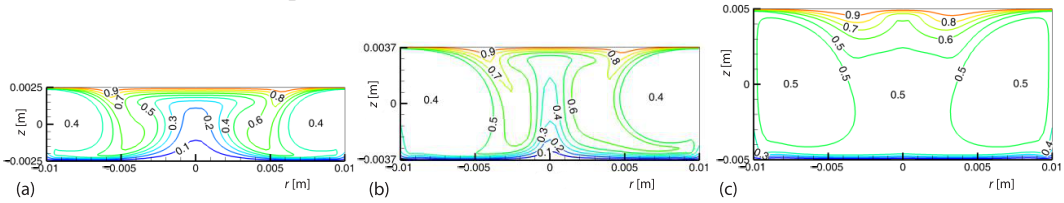


**Figure 10. The Si concentration distribution on the meridian plane $\theta = \pi/2$; (a) $As = 0.5$, (b) $As = 0.75$, and (c) $As = 1$**

As previously mentioned, vortices are formed in both axial and circumferential directions of the liquid bridge after the surface tension flow changes to a 3-D convection model. Figure 11 shows tangential velocity distribution on the free surface $R = 10$ mm, which can be seen that the circumferential flow exhibits a convective structure with azimuthal wave number $m$. The azimuthal wavenumber $m$ decreases from 4 to 2 when aspect ratio increases from 0.5-1. In addition, tangential velocity isoline on the free surface is substantially parallel to the axial direction except the regions near upper and lower surfaces, indicating that convection in the liquid bridge presents a 3-D global vortex convection structure.

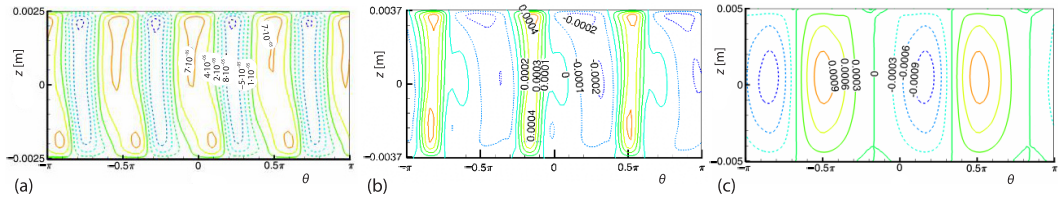


**Figure 11. Tangential velocity distribution on the free surface $R = 10$ mm; (a) $As = 0.5$ (b) $As = 0.75$, and (c) $As = 1$**

Figure 12 shows that isotherms are basically parallel on the free surface. The temperature on the free surface is approximately linearly distributed with the axial height of the liquid bridge. This phenomenon is due to the relatively large heat diffusion capacity of the low-Pr fluid. Temperature gradient is relatively large in the local regions near the boundary of high and low temperature. Since fluid transports from the hot end to the cold end along the free surface, temperature gradient along the fluid-flow decreases slightly on the free surface. Generally speaking, azimuthal wavenumber varies with aspect ratio. However, at the same level, there is only a slight fluctuation in temperature distribution on the free surface. Heat transport along the axis of the liquid bridge is still dominated by thermal diffusion.

Concentration distribution on free surface with $R = 10$ mm is related to azimuthal wavenumber under different aspect ratios. Concentration isolines are wavy lines near the high temperature surface. The larger of aspect ratio, the wider of the wavy line region. Concentration isolines exhibit a string of vertical stripes in other regions of free surface. Therefore, concentration gradient near the low temperature surface is the largest. The result is shown in fig. 13.

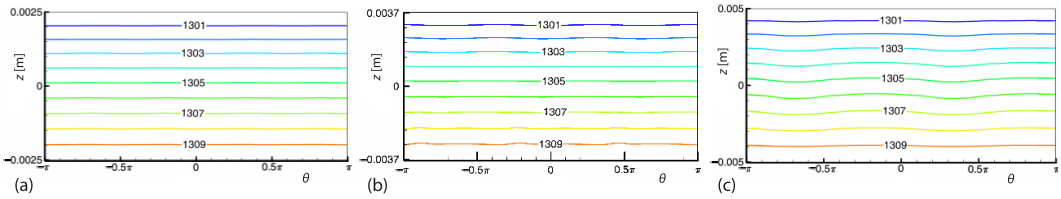


**Figure 12. Temperature distribution on the free surface with $R$ =10 mm; (a) $As$ = 0.5, (b) $As$ = 0.75, and (c) $As$ = 1**

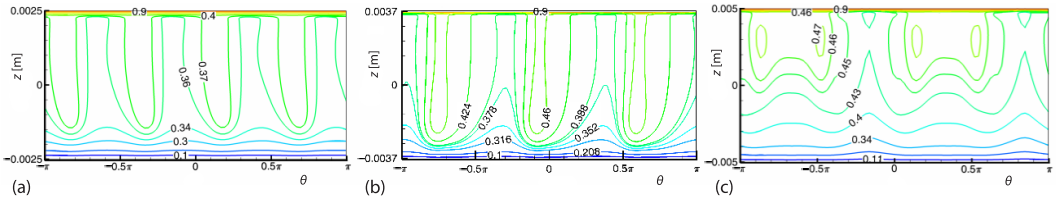


**Figure 13. Concentration distribution on the free surface with $R$ = 10 mm; (a) $As$ = 0.5, (b) $As$ = 0.75, and (c) $As$ = 1**

Figure 14 shows time dependency of velocity and concentration for the monitoring point $p(r = R, \theta = 0, z = 0)$ at different aspect ratios. Velocity and concentration no longer change with time after initial short-term oscillation at $As$ = 1, while $As$ < 1, both monitoring point velocity and concentration periodically oscillate with time. Amplitude of the monitoring point at $As$ = 0.75 is larger than that at $As$ = 0.5, but frequency is smaller than that at $As$ = 0.5. As aspect ratio increases, average velocity of the monitoring points decreases, and corresponding average concentration increases conversely. This can be explained by the fact that larger velocity causes more melt at a lower concentration delivered, and thus concentration is lowered.

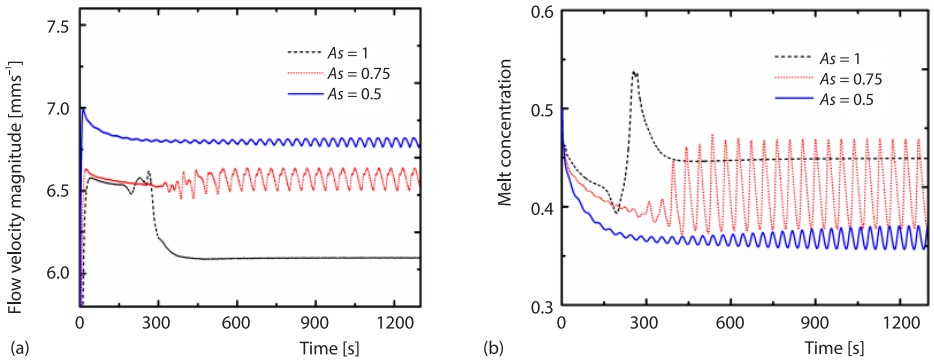


**Figure 14. Time dependency of velocity with time (a) and Si concentration (b) at different aspect ratio**

Figure 15 shows time dependency of velocity and melt concentration and fast Fourier transform spectrum analysis at $As$ = 0.75. Oscillation frequency is $f$ = 0.0216 Hz and corresponding period is $\tau$ = 46.3 seconds. Oscillation frequency of the monitoring point at $As$ = 0.75 is lower than that at $As$ = 0.5. It is reasonable to believe that concentration oscillation is caused by velocity oscillation. At the same time, change in concentration also causes change of surface solute capillary force, thereby changing velocity of the capillary flow. Therefore, changes in both concentration and velocity are coupled together. As shown in fig. 15(a), roughly, when velocity of the monitoring point is large, corresponding concentration is also high at that mo-

ment, but the phases of concentration and velocity are not completely synchronized. This phenomenon is different from the conclusion that concentration decreases with increase of velocity at different aspect ratios, which again reflects result of coupling of velocity and concentration.

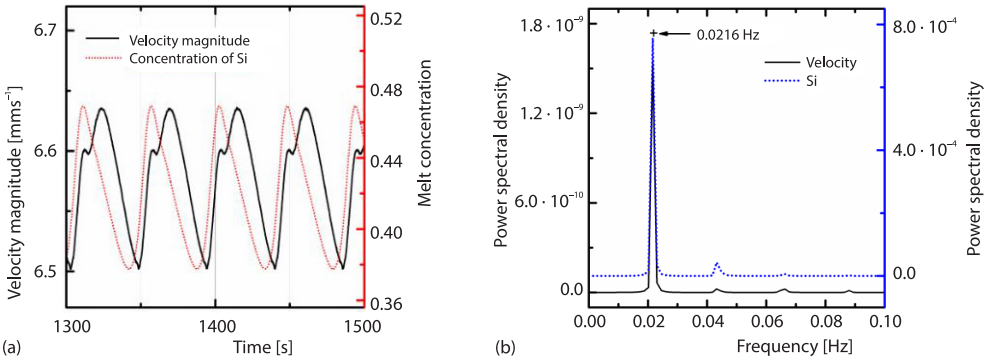


**Figure 15. Time dependency of velocity and concentration (a) and frequency spectrum (b) at *As* = 0.75**

## Conclusions

Various capillary convection characteristics in a half-floating zone liquid bridge with a radius of 10 mm were analyzed and effects of aspect ratio on stability of coupled solute-thermocapillary convection and concentration field were also studied. Some results have been found.

- For *As* = 0.5, when pure solute capillary convection with a 2-D axisymmetric structure is added to pure thermocapillary convection with a 3-D steady non-axisymmetric model, coupled solute-thermocapillary convection exhibits a 3-D periodic and rotating oscillatory flow pattern. Weak solute convection causes a large change in stability of thermocapillary convection. Further analysis reveals that when velocity of the monitoring point is large, corresponding concentration is also high at that moment, but the phases of concentration and velocity are not completely synchronized.
- For *As* = 0.75, periodic oscillation frequency of velocity and concentration of the monitoring point is 0.0216 Hz which is lower than that at *As* = 0.5 with value of 0.0302 Hz. But comparing with *As* = 0.5, amplitude of the monitoring point is larger. After initial short-term irregular oscillation, velocity and concentration of the monitoring point no longer change with time while *As* = 1. Meanwhile, with increase of aspect ratio, average velocity of monitoring point decreases, and corresponding average concentration increases. When values 0.5, 0.75, and 1 are employed for aspect ratio, azimuthal wavenumber m is 4, 3, and 2, respectively. Product of azimuthal wavenumber and aspect ratio is a value between 2 and 2.2, which is similar to the previous results for the case of pure thermal Marangoni convection.

## Acknowledgment

This work is supported by the National Natural Science Foundation of China (Grant Nos. 51976080, 11474003, and 11675077), University Natural Science Research Project of Anhui Province (Grant Nos. KJ2019ZD06, KJ2021A0388) and Natural Science Foundation of Anhui Province (Grant Nos. 1908085MF197, 2008085QF313).

## References

[1] Granata, V., *et al*., Crystal Growth of the $Ca_2RuO_4$-Ru Metal System by the Floating-Zone Technique, *Journal of Alloys and Compounds*, *832* (2020), 154890

[2] Agamaliyev, Z. A., *et al.*, A Model for Crystal Growth of Solid Solutions in the InAs-GaAs System by a Modified Floating-Zone Technique, *Inorganic Materials*, *55* (2019), 3, pp. 205-209
[3] Muiznieks, A.*, et al.*, *7 - Floating Zone Growth of Silicon A2*, in: *Handbook of Crystal Growth* , 2nd ed., (Ed., P. Rudolph), Elsevier, Boston, Mass., USA, 2015, pp. 241-279
[4] Han, X.-F., *et al*., Numerical Analysis of Dopant Concentration in 200 mm (8 inch) Floating Zone Silicon, *Journal of Crystal Growth*, *545* (2020), 125752
[5] Tsukada, T., The 22 – *The Role of Marangoni Convection in Crystal Growth A2 in: Handbook of Crystal Growth*, 2nd ed., (Ed., P. Rudolph), Elsevier, Boston, Mass., USA, 2015, pp. 871-907
[6] Yang, S., *et al*., The Effect of Uniform Magnetic Field on Spatial-Temporal Evolution of Thermocapillary Convection with the Silicon Oil Based Ferrofluid, *Thermal Science*, *24* (2020), 6B, pp. 4159-4171
[7] Melnikov, D. E., *et al.*, Modelling of the Experiments on the Marangoni Convection in Liquid Bridges in Weightlessness for a Wide Range of Aspect Ratios, *International Journal of Heat and Mass Transfer*, *87* (2015), Aug., pp. 119-127
[8] Schwabe, D., *et al*., Oscillatory Thermocapillary Convection in Open Cylindrical Annuli – Part 1: Experiments under Microgravity, *Journal of Fluid Mechanics*, *491* (2003), Sept., pp. 239-258
[9] Takagi, K., *et al*., Experimental Study on Transition Oscillatory Thermocapillary Flow in a Low Prandtl Number Liquid Bridge, *Journal of Crystal Growth*, *233* (2001), 1, pp. 399-407
[10] Yang, S., *et al.*, A New Cognition on Oscillatory Thermocapillary Convection for High Prandtl Number Fluids, *Thermal Science*, *25* (2021), 6B, pp. 4761-4772
[11] Jayakrishnan, R., Tiwari, S., Influence of co-Axial Air-Flow and Volume Ratio on Thermo-Capillary Convection in Half Floating Zones, *Computers & Fluids*, *179* (2019), Jan., pp. 248-264
[12] Smith, M. K., Davis, S. H., Instabilities of Dynamic Thermocapillary Liquid Layers – Part 1: Convective Instabilities, *Journal of Fluid Mechanics*, *132* (1983), July, pp. 119-144
[13] Smith, M. K., Davis, S. H., Instabilities of Dynamic Thermocapillary Liquid Layers – Part 2: Surface-Wave Instabilities, *Journal of Fluid Mechanics*, *132* (1983), July, pp. 145-162
[14] Lyubimova, T. P., *et al*., Thermo- and Soluto-Capillary Convection in the Floating Zone Process in Zero Gravity Conditions, *Journal of Crystal Growth*, *303* (2007), 1, pp. 274-278
[15] Lyubimova, T. P., Scuridyn, R. V., Numerical Modelling of 3-D Thermo- and Solutocapillary-Induced Flows in a Floating Zone during Crystal Growth, *The European Physical Journal Special Topics*, *192* (2011), 1, pp. 41-46
[16] Minakuchi, H., *et al*., A 3-D Numerical Simulation Study of the Marangoni Convection Occurring in the Crystal Growth of $SixGe_{1-x}$ by the Float-Zone Technique in Zero Gravity, *Journal of Crystal Growth*, 266 (2004), 1, pp. 140-144
[17] Minakuchi, H., *et al.*, The Relative Contributions of Thermo-Solutal Marangoni Convections on Flow Patterns in a Liquid Bridge, *Journal of Crystal Growth*, *385* (2014), Jan., pp. 61-65
[18] Minakuchi, H., *et al*., Effect of Thermo-Solutal Marangoni Convection on the Azimuthal Wave Number in a Liquid Bridge, *Journal of Crystal Growth*, *468* (2017), June, pp. 502-505
[19] Surovovs, K., *et al*., Hydrodynamical Aspects of the Floating Zone Silicon Crystal Growth Process, *Journal of Crystal Growth*, *401* (2014), Sept., pp. 120-123
[20] Zhou, X. M., Huai, X. L., Free Surface Deformation of Thermo-Solutocapillary Convection in Axisymmetric Liquid Bridge, *Microgravity Science And Technology*, *27* (2015), 1, pp. 39-47
[21] Chen, J.-C., *et al*., The 3-D Numerical Simulation of Pure Solutocapillary Flow in a Shallow Annular Pool for Mixture Fluid with High Schmidt Number, *Microgravity Science and Technology*, *28* (2016), 1, pp. 49-57
[22] Huang, H., *et al*., Effect of Marangoni Number on Thermocapillary Convection in a Liquid Bridge under Microgravity, *International Journal of Thermal Sciences*, *118* (2017), Aug., pp. 226-235
[23] Mendis, R. L. A., *et al.*, The Relative Contribution of Solutal Marangoni Convection Thermal Marangoni Flow Instabilities in a Liquid Bridge of Smaller Aspect Ratios under Zero Gravity, *Crystals*, *11* (2021), 2, 116
[24] Mendis, R. L. A., *et al*., Global Linear Stability Analysis of Thermo-solutal Marangoni Convection in a Liquid Bridge under Zero Gravity, *Microgravity Science and Technology*, *32* (2020), 4, pp. 729-735
[25] Liang, R., *et al*., Effect of Horizontal Vibrations on Thermo-Solutocapillary Convection and Free Surface of Liquid Bridge, *Microgravity Science and Technology*, *32* (2020), 5, pp. 847-855
[26] Campbell, T. A., *et al.*, Float Zone Growth and Characterization of $Ge_{1-x}Si_x$ ($x \leq 10$ at %) Single Crystals, *Journal of Crystal Growth*, *226* (2001), 2, pp. 231-239
[27] Abbasoglu, S., Sezai, I., 3-D Modelling of Melt Flow and Segregation during Czochralski Growth of $Ge_xSi_{1-x}$ Single Crystals*, International Journal of Thermal Sciences*, *46* (2007), 6, pp. 561-572

[28] Fadaly, E. M. T.*, et al.*, Direct-Bandgap Emission from Hexagonal Ge and SiGe Alloys*, Nature*, *580* (2020), 7802, pp. 205-209
[29] Zou, Y., *et al*., Instability of Coupled Thermo-Solute Capillary Convection in Liquid Bridge and Control by Rotating Magnetic Field (in Chinese), *Lixue Xuebao/Chinese Journal of Theoretical and Applied Mechanic*s, *49* (2017), 6, pp. 1280-1289
[30] Levenstam, M., Amberg, G., Hydrodynamical Instabilities of Thermocapillary Flow in a Half-Zone, *Journal of Fluid Mechanics*, *297* (1995), Aug., pp. 357-372
[31] Zou, Y., *et al*., Effect of Rotating Magnetic Field on Thermal Convection and Dopant Transport in Floating-Zone Crystal Growth, *Microgravity Science and Technology*, *32* (2020), 3, pp. 349-361
[32] Preisser, F., *et al*., Steady and Oscillatory Thermocapillary Convection in Liquid Columns with Free Cylindrical Surface, *Journal of Fluid Mechanics*, *126* (1983), Jan., pp. 545-567
[33] Wanschura, M., *et al*., Convective Instability Mechanisms in Thermocapillary Liquid Bridges, *Physics of Fluids*, *7* (1995), 5, pp. 912-925

Paper submitted: June 11, 2021
Paper revised: February 16, 2022
Paper accepted: June 13, 2022